Estimating the velocity profile and acoustical quantities of a harmonically vibrating loudspeaker membrane from on-axis pressure data*

Ronald M. Aarts[1,2], *AES fellow*, and Augustus J.E.M. Janssen[1]

[1]Philips Research Laboratories,

HTC 36, 5656AE Eindhoven, The Netherlands

[2]Technical University Eindhoven, Den Dolech 2,

P.O Box 513, NL-5600 MB Eindhoven, The Netherlands

October 26, 2009

Abstract

Formulas are presented for acoustical quantities of a harmonically excited resilient, flat, circular loudspeaker in an infinite baffle. These quantities are the sound pressure on-axis, far-field, directivity, and the total radiated power.

*Paper 7678 Presented at the 126th Convention 2009 May 7–10 Munich, Germany

These quantities are obtained by expanding the velocity distribution in terms of orthogonal polynomials. For rigid and non-rigid radiators, this yields explicit, series expressions for both the on-axis and far-field pressure. In the reverse direction, a method of estimating velocity distributions from (measured) on-axis pressures by matching in terms of expansion coefficients is described. Together with the forward far-field computation scheme, this yields a method for assessment of loudspeakers in the far-field and of the total radiated power from (relatively near-field) on-axis data (generalized Keele scheme).

0 Introduction

In this paper an analytic method developed in [1, 2] for the calculation of acoustical quantities such as the sound pressure on-axis, far-field, directivity, and the total radiated power is presented to the audio engineering community. This method is based on the analytical results as developed in the diffraction theory of optical aberrations by Nijboer [3] and Zernike and Nijboer [4], see also [5, 6]. Using this approach, many of the analytic results in Greenspan [7], such as those on the sound pressure on-axis, the total radiated power, and the results in text books [8] on far-field expressions and directivity can be presented and extended in a systematic fashion. This is worked out in [1] for the results on on-axis pressure and far-field expressions for arbitrary velocity distributions on flat piston radiators. The mathematical foundation of these methods related to directivity, and the total radiated power is discussed in [2]. An arbitrary

velocity distribution can be efficiently developed as a series in Zernike polynomials. Using near-field pressure measurements on-axis the coefficients of these polynomials can be estimated. With these estimated coefficients the acoustical quantities mentioned above can be estimated as well. An immediate application is to predict far-field sound pressure data from near-field pressure data measured without using an anechoic chamber (generalized Keele scheme [1, 9]).

The radiated pressure is given in integral form by the Rayleigh integral [8, 10] as

$$p(\underline{r},t) = \frac{i\rho_0 ck}{2\pi}\, e^{i\omega t} \int_S v(\underline{r}_s)\, \frac{e^{-ikr'}}{r'}\, dS \ , \tag{1}$$

where ρ_0 is the density of the medium, c is the speed of sound in the medium, $k = \omega/c$ is the wave number and ω is the radian frequency of the harmonically vibrating surface S. Furthermore, t is time, $\underline{r}$ is a field point, $\underline{r}_s$ is a point on the surface S, $r' = |\underline{r} - \underline{r}_s|$ is the distance between $\underline{r}$ and $\underline{r}_s$, and $v(\underline{r}_s)$ is the normal component of a (not necessarily uniform) velocity profile on the surface S. The time variable t in $p(\underline{r},t)$ and the harmonic factor $\exp(i\omega t)$ in front of the integral in Eq. (1) will be omitted in the sequel. For transparency of exposition, the surface S is assumed [1, 2] to be a disk of radius a, $|\underline{r}_s| = r_s \leq a$, with average velocity V_s; in [1] a generalization to the case of dome-shaped radiator surfaces S is done. In [11] a generalization for a loudspeaker modelled as a resilient spherical cap on a rigid sphere is presented. See Fig. 1 for the geometry and notations used in the case of a flat piston. The volume velocity V at the piston is

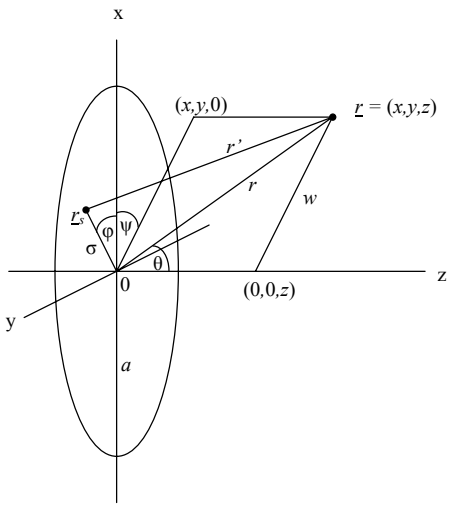

Figure 1: Set-up and notations.

$$
\begin{aligned}
\underline{r}_s &= (x_s, y_s, 0) = (\sigma\cos\varphi, \sigma\sin\varphi, 0) \\
\underline{r} &= (x, y, z) = (r\sin\theta\cos\psi, r\sin\theta\sin\psi, r\cos\theta) \\
w &= r\sin\theta = (x^2+y^2)^{1/2}, \quad z = r\cos\theta \\
r &= |\underline{r}| = (x^2+y^2+z^2)^{1/2} = (w^2+z^2)^{1/2} \\
r' &= |\underline{r} - \underline{r}_s| = (r^2+\sigma^2-2\sigma w\cos(\psi-\varphi))^{1/2}.
\end{aligned}
$$

$$V = \int_S v(\underline{r}_s)\, dS = V_s \pi a^2. \tag{2}$$

Frankort [12] has shown that loudspeaker cones mainly vibrate in a radially symmetric fashion. This is in general certainly not the case for all loudspeakers– the limitation is further discussed in Sec. 6–but our attention in this paper is restricted to radially symmetric velocity distributions v, which are denoted as $v(\sigma), 0 \leq \sigma \leq a$. Define the Zernike terms [3, 4]

$$R^0_{2n}(\rho) = P_n(2\rho^2 - 1)\ , \quad 0 \leq \rho \leq 1\ , \tag{3}$$

where P_n are the Legendre polynomials [13]. By completeness and orthogonality (see Eq. (9)), the velocity profile $v(\sigma)$ admits the representation

$$v(\sigma) = V_s \sum_{n=0}^{\infty} u_n R^0_{2n}(\sigma/a)\ , \quad 0 \leq \sigma \leq a\ , \tag{4}$$

in which u_n are scalar coefficients (see Eq. (5)). In [1] there are presented analytical results for the on-axis and far-field pressure $p(\underline{x})$ in Eq. (1) related to the coefficients u_n and polynomials R^0_{2n} occurring in the expansion in Eq. (4).

By orthogonality of the terms $R^0_{2n}(\rho)$, the coefficients u_n in Eq. (4) can be found in integral form as

$$u_n = \frac{2(2n+1)}{V_s} \int_0^1 R^0_{2n}(\rho) v(a\rho) \rho d\rho\ , \quad n = 0, 1, \cdots\ . \tag{5}$$

In particular, $u_0 = 1$. There is an impressive number of cases where one can explicitly find the u_n in Eq. (5); these include the rigid piston ($\ell = 0$), the simply supported radiator ($\ell = 1$) and the higher order clamped radiators ($\ell \geq 2$) with

the velocity profile of Stenzel [14] given in Greenspan's notation [7] as

$$v^{(\ell)}(\sigma) = (\ell+1)V_s(1-(\sigma/a)^2)^\ell H(a-\sigma)\ , \qquad \ell = 0, 1, \cdots \quad , \tag{6}$$

and the Gaussian velocity profile

$$v(\sigma;\alpha) = \frac{\alpha V_s}{1-e^{-\alpha}} e^{-\alpha(\sigma/a)^2} H(a-\sigma)\ , \tag{7}$$

where $H(x)$ is the Heaviside function, $H(x) = 0,\ 1/2,$ or 1 according as x is negative, zero, or positive. Hence, the velocity profiles in Eqs. (6) and (7) vanish for $\sigma > a$. This is illustrated in Fig. 2 where various profiles are plotted.

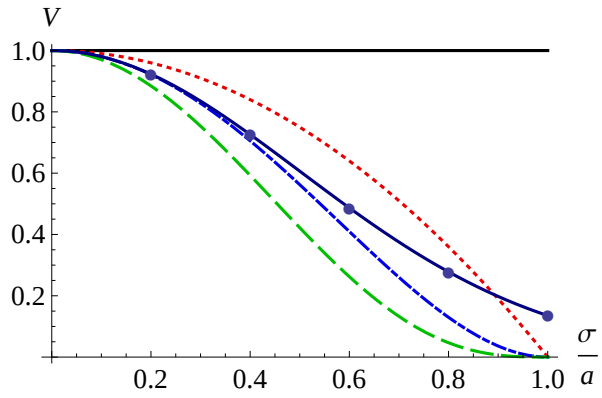

Figure 2: Normalized velocity profiles V for the rigid piston ($\ell = 0$) (solid curve), the simply supported radiator ($\ell = 1$) (dotted curve) and the first two clamped radiators ($\ell = 2, 3$) (dash-dotted and dashed curves, respectively) using Eq. (6), and the truncated Gaussian profile ($\alpha = 2$, solid curve with closed circles) using Eq. (7). The normalization is such that the velocity is equal to 1 at $\sigma/a = 0$. The velocity is equal to zero for $|\sigma/a| > 1$.

The relevance of the Zernike terms R_{2n}^0 for the purposes of the present paper is the existence of closed-form formulas. For instance, the radiators in Eq. (6) give rise to an on-axis pressure expansion in the form of a series of $n+1$ terms $u_\ell j_\ell(kr_-)h_\ell^{(2)}(kr_+)$, with $r_\pm$ argument values directly related to the axial position $(0,0,r)$, while the far-field pressure expansion is a similar series involving terms $u_\ell J_{2\ell+1}(ka\sin\theta)/(ka\sin\theta)$. In [2] it is shown how the acoustic power P and the directivity D are computed from the coefficients u_ℓ. In the reverse direction, the forward computation schemes for the on-axis and far-field pressures is complemented in [1] by an inverse method with potential use in far-field loudspeaker assessment. Here one estimates the expansion coefficients u_n of a velocity profile v by matching with a measured on-axis pressure data set and then one predicts the far-field sound radiation using the far-field forward formula.

1 Paper outline

In Sec. 2 the definition and basic properties of the Zernike polynomials are given, and some of the expansion results that are relevant for this paper are presented. Furthermore, the Hankel transform of the Zernike polynomials is presented in closed form. The latter result is of importance both for the forward computation scheme for the far-field and for establishing results on the radiated power, etc.

In Sec. 3 the basic formulas are highlighted and discussed. Thus, the closed form involving a spherical Bessel and Hankel function for the on-axis pressure

associated with a single Zernike term is presented, with comments on both near-field and far-field behavior and on behavior for low and high frequencies in terms of ka. Also the far-field expression is presented as derived in [1].

In Sec. 4, the formulas [2] for the total radiated power and directivity, are presented and discussed.

In Sec. 5 the inverse method [1] of estimating the Zernike expansion coefficients of the velocity profile from the on-axis (measured, sampled) pressure data is considered. Together with the forward scheme for computing far-field pressures from Zernike expansions, this yields a loudspeaker assessment method that generalizes a well-known method in audio engineering for estimating the far-field of a loudspeaker from near-field on-axis data in the case of a rigid piston (Keele scheme [9]).

In the present paper only a few measurements and simulation results will be shown.

2 The Zernike terms R_{2n}^0

The Zernike terms R_{2n}^0 are polynomials of degree $2n$ given by

$$R_{2n}^0(\sigma/a) = P_n(2(\sigma/a)^2 - 1) = \sum_{s=0}^{n}(-1)^s \binom{2n-s}{n} \binom{n}{s} (\sigma/a)^{2n-2s} \quad , \tag{8}$$

where P_n is the Legendre polynomial of degree n, see Ref. [13, 22.3.8 and 22.5.42]. The first few R_{2n}^0 are given in Table 1, and in Fig. 3 some of them are plotted as a function of $\rho = \sigma/a \ \in [0, 1]$. The R_{2n}^0 cannot be interpreted

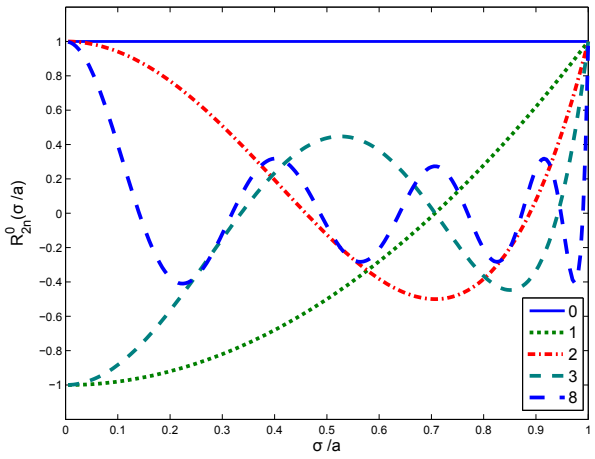

Figure 3: The Zernike terms R^0_{2n} vs. σ/a for $n = 0, 1, 2, 3$ and $n = 8$; note the increasing number of undulations for increasing n.

directly in physical terms, unlike the velocity profiles $v^{(\ell)}$ in Eq. (6) in which ℓ has the interpretation of a smoothness parameter for the transition from the non-zero values on the piston ($\sigma < a$) to the value zero outside the piston ($\sigma > a$). Rather, their significance for loudspeaker analysis stems from the following facts.

- They are very efficient and convenient in representing a general velocity profile v. This is due to the orthogonality property

$$\int_0^1 R^0_{2n_1}(\rho)\, R^0_{2n_2}(\rho)\, \rho\, d\rho \;=\; \begin{cases} \frac{1}{2(2n_1+1)} & , n_1 = n_2 \;, \\ 0 & , n_1 \neq n_2 \;, \end{cases} \tag{9}$$

  as well as the fact that many velocity profiles considered in loudspeaker analysis can be represented as a Zernike series. In [1][Appendix A], a number of cases are listed, such as the expansions for the velocity profiles

in Eq. (6) and Eq. (7).

- The Hankel transform of 0^{th} order of the R_{2n}^0 has a closed form, viz.

$$\int_0^a J_0(u\sigma) R_{2n}^0(\sigma)\sigma d\sigma = (-1)^n \frac{a}{u} J_{2n+1}(ua) \; . \tag{10}$$

This formula has been proved in Ref. [3] as a special case of a formula expressing the m^{th} order Hankel transform of Zernike polynomials of azimuthal order m in terms of Bessel functions of the first kind. This formula is very important for the development of explicit analytic results in the spirit of [7]. It gives for instance, the far-field expression for the pressure due to a single term R_{2n}^0 in the velocity profile, see Sec. 3.2 and [1][Appendix B].

Table 1: Zernike polynomials

n	$R_{2n}^0(\sigma/a)$
0	1
1	$2(\sigma/a)^2 - 1$
2	$6(\sigma/a)^4 - 6(\sigma/a)^2 + 1$
3	$20(\sigma/a)^6 - 30(\sigma/a)^4 + 12(\sigma/a)^2 - 1$

3 On-axis and far-field expressions

The velocity profile $v(\sigma)$ considered in this section (normal component) vanishes outside the disk $\sigma \leq a$ and has been developed into a Zernike series as in Eq. (4) with coefficients u_n given in accordance with Eq. (5) or explicitly as in the cases discussed earlier.

3.1 On-axis expression

There holds [1] for an on-axis point $\underline{r} = (0, 0, r)$ with $r \geq 0$ the formula

$$p(\underline{r}) = \frac{1}{2} V_s \rho_0 c (ka)^2 \sum_{n=0}^{\infty} \gamma_n(k, r) u_n \ , \tag{11}$$

in which

$$\begin{aligned} &\gamma_n(k, r) = (-1)^n j_n(kr_-) h_n^{(2)}(kr_+) \ , \\ &r_\pm = \tfrac{1}{2}(\sqrt{r^2 + a^2} \pm r) \ . \end{aligned} \tag{12}$$

The $r_\pm$ in Eq. (12) satisfy

$$\begin{aligned} &0 \leq r_- \leq \tfrac{1}{2} a \leq r_+ \ , \ \ r_+ r_- = \tfrac{1}{4} a^2 \ , \\ &r_+ + r_- = \sqrt{r^2 + a^2} \ . \end{aligned} \tag{13}$$

The j_n and $h_n^{(2)} = j_n - i\, y_n$ are the spherical Bessel and Hankel function, respectively, of the order $n = 0, 1, \cdots$, see Ref. [13, § 10.1.]. In particular, $j_0(z) = (\sin z)/z$ and $h_0^{(2)}(z) = (ie^{-iz})/z$.

Figure 4 shows a plot of $|\gamma_{\ell=n=0}(k, r)|$ as a function of r/a (rigid piston) and of $|\gamma_n(k, r)|$ for $n = 1, 2, 3$. Some comments on these plots are presented at the end of this subsection.

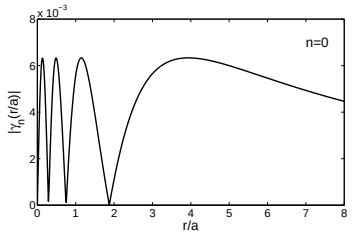

(a)

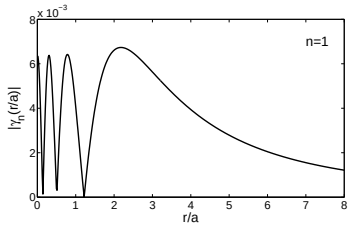

(b)

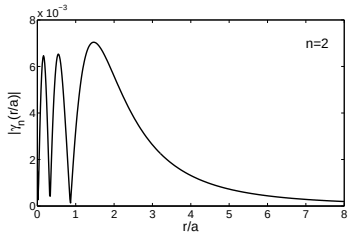

(c)

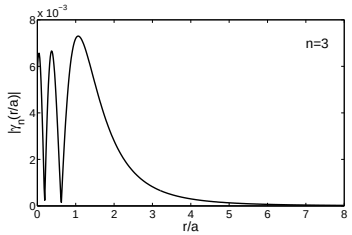

(d)

Figure 4: The product $|j_n(kr_-)\, h_n^{(2)}(kr_+)|$ from Eq. (12), for $n = 0, \ldots, 3$, vs. r/a, where $a/\lambda = 4$, and $a = 0.1$ m, which yields $f = 13.7$ kHz and $ka = 8\pi$. (a) $n = 0$, (b) $n = 1$, (c) $n = 2$, (d) $n = 3$.

The result in Eqs. (11) and (12) comprises the known result [8, 8.31a,b] for the rigid piston with $p(\underline{r})$, $\underline{r} = (0, 0, r)$, given by

$$\begin{aligned} p(\underline{r}) &= \tfrac{1}{2} V_s \rho_0 c (ka)^2 \tfrac{\sin kr_-}{kr_-} \tfrac{ie^{-ikr_+}}{kr_+} \\ &= 2i\rho_0 c V_s e^{-\frac{1}{2}ik((r^2+a^2)^{\frac{1}{2}}+r)} \cdot \\ &\quad \sin(\tfrac{1}{2}k((r^2+a^2)^{\frac{1}{2}} - r)) \ , \end{aligned} \tag{14}$$

and it generalizes immediately to the case of the simply supported radiator ($\ell = 1$) and the clamped radiators.

In Fig. 5 the rigid piston ($\ell = 0$), the simply supported radiator ($\ell = 1$) and the first two clamped radiators ($\ell = 2, 3$) are considered ($|p(\underline{r})|$, normalized as a function of r/a).

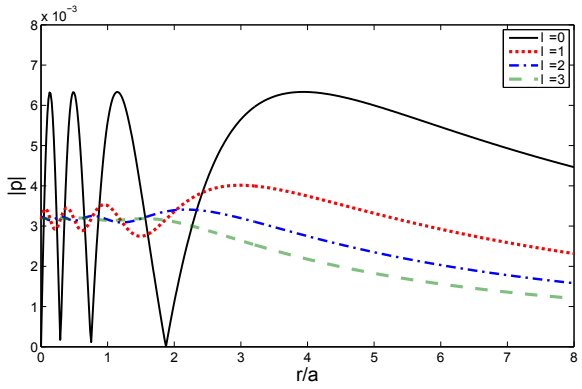

Figure 5: Normalized $|p|$ vs. r/a for the rigid piston ($\ell = 0$) (solid curve), the simply supported radiator ($\ell = 1$) (dotted curve) and the first two clamped radiators ($\ell = 2, 3$) (dash-dotted and dashed curves, respectively) using Eq. (11). Here $a/\lambda = 4$ and $ka = 8\pi$. The normalization is equal to $(\ell + 1)/2\ \rho_0 c V_s (ka)^2$. The factor $\ell + 1$ allows an easier comparison of the four curves.

The next comments concern the behavior of the terms γ_n in Eq. (12). From Eqs. (12)–(13) it follows that

$$r_- \approx \frac{1}{2}(a-r) \approx \frac{1}{2}a \approx \frac{1}{2}(a+r) \approx r_+ \ , \quad r \ll a \ . \tag{15}$$

Therefore, when ka is large and $r \to 0$ (with n not large), it follows from the results in Ref. [13], Sec. 10.1 that

$$|\gamma_n(k,r)| \approx \frac{|\cos \frac{1}{2}k(a-r)|}{\frac{1}{4}k^2a^2} \ , \tag{16}$$

confirming the presence of zeros and the largely n-independent envelope of the curves in Fig. 4 near $r = 0$.

Finally, when $r \gg a$ it follows from Eqs. (12)–(13) that

$$r_- \approx \frac{a^2}{4r} \ , \quad r_+ \approx r \ . \tag{17}$$

Therefore, from Ref. [13], Sec. 10.1,

$$\gamma_n(k,r) \approx \frac{(\frac{-ika^2}{4r})^n}{1 \cdot 3 \cdot \cdots \cdot (2n+1)} \frac{e^{-ikr_+}}{-ikr_+} \tag{18}$$

which shows an $O(1/r^{n+1})$-behavior of $\gamma_n(k,r)$ as $n \to \infty$.

3.2 Far-field expression

Using the Zernike expansion Eq. (4) of $v(\sigma)$ it is shown in [1][Appendix B] that the following far-field approximation holds: when $\underline{r} = (r\sin\theta, 0, r\cos\theta)$ and $r \to \infty$,

$$p(\underline{r}) \approx i\rho_0 ckV_s \frac{e^{-ikr}}{r} a^2 \sum_{n=0}^{\infty} u_n (-1)^n \frac{J_{2n+1}(ka\sin\theta)}{ka\sin\theta} \ . \tag{19}$$

In the case of a rigid piston, it follows that

$$p(\underline{r}) \approx i\rho_0 ckV_s \frac{e^{-ikr}}{r} \frac{J_1(ka\sin\theta)}{ka\sin\theta} \quad . \tag{20}$$

This is the familiar result for the far-field pressure of a rigid piston as can be found in the textbooks, see, e.g., Kinsler et al. [8, (8.35)]. In Fig. 6 a plot can be found of $|\frac{J_{2n+1}(ka\sin\theta)}{ka\sin\theta}|$, $n = 0, 1, 2, 3$, as a function of $ka\sin\theta$.

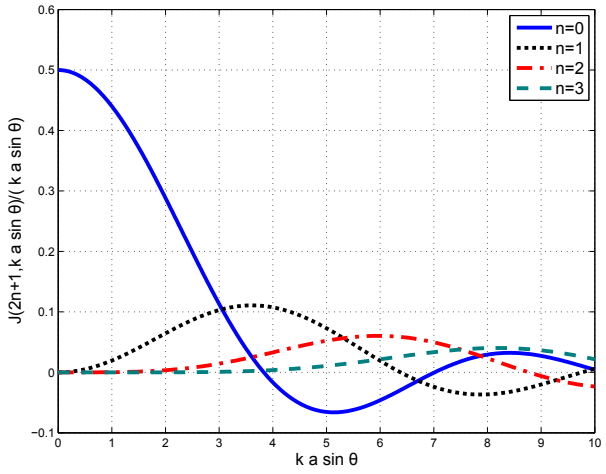

Figure 6: $|\frac{J_{2n+1}(ka\sin\theta)}{ka\sin\theta}|$ vs. $ka\sin\theta$.

For the simply supported radiator, case $\ell = 1$ in Eq. (6), and for the clamped radiators, cases $\ell \geq 2$ in Eq. (6), the coefficients u in the Zernike expansion of the $v^{(\ell)}$ in Eq. (6) are available [1, Appendix A] and this gives the far-field approximation of $p(\underline{r})$ via Eq. (19).

Some comments on the behavior of the terms $J_{2n+1}(z)/z$, $z = ka\sin\theta$, as they occur in the series in Eq. (19) are presented now. From the asymptotics of the Bessel functions, as given in Ref. [13, Eq. 9.3.1], it is seen that in the series in Eq. (19) only those terms contribute significantly for which $2n+1 \leq \frac{1}{2}e\ ka\sin\theta$.

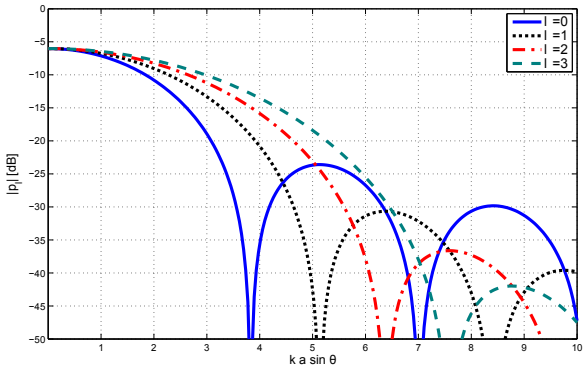

Figure 7: Normalized $|p|$ vs. $ka\sin\theta$, using the Zernike expansion of the $v^{(\ell)}$ and Eq. (19).

In particular, when $\theta = 0$, it is only the term with $n = 0$ that is non-vanishing, and this yields

$$p((0,0,r)) \approx \frac{1}{2} i\rho_0 c V_s ka^2 \frac{e^{-ikr}}{r} \ , \quad r \to \infty \ . \tag{21}$$

This is in agreement with what is found from Eq. (11) when only the term with $n = 0$ is retained and r_+ is replaced by r, r_- is replaced by 0. For small values of ka the terms in the series Eq. (19) decay very rapidly with n. For large values of ka, however, a significant number of terms may contribute, especially for angles θ far from 0.

4 Power output and directivity

The power is defined as the intensity pv^* (where * denotes the complex conjugate) integrated over the plane $z = 0$. Thus, because v vanishes outside S,

$$P = \int_S p(\sigma) v^*(\sigma) dS \ , \tag{22}$$

where $p(\sigma) = p((\sigma\cos\psi, \sigma\sin\psi, 0))$ is the pressure at an arbitrary point on S. In [2], Sec. V it is shown from Kings's result [15] that

$$P = 2\pi i\rho_0 ck \int_0^\infty \frac{V(u)V^*(u)}{(u^2-k^2)^{1/2}} u du \ , \tag{23}$$

where

$$V(u) = \int_0^a J_0(u\sigma)\, v(\sigma)\, \sigma\, d\sigma \ , \qquad u \geq 0 \ , \tag{24}$$

is the Hankel transform of v. This gives rise, via Eqs. (4) and (10), to the integrals

$$\int_0^\infty \frac{J_{2n_1+1}(au)J_{2n+1}(au)}{(u^2-k^2)^{1/2}} du \ . \tag{25}$$

and these have been evaluated in the form of a power series in ka in [2][Sec.V.B].

We next consider the directivity. With the usual approximation arguments in the Rayleigh integral representation of p in Eq. (1)

there follows ($\underline{r} = (r\cos\psi\sin\theta, r\sin\psi\sin\theta, r\cos\theta)$)

$$p(\underline{r}) \approx i\rho_0 ck \frac{e^{-ikr}}{r} V(k\sin\theta) \ . \tag{26}$$

From this there results the directivity

$$\begin{aligned} D &= \frac{4\pi|V(0)|^2}{\int_0^{2\pi}\int_0^{\pi/2} |V(k\sin\theta)|^2 \sin\theta d\psi d\theta} \\ &= \frac{2|V(0)|^2}{\int_0^{\pi/2} |V(k\sin\theta)|^2 \sin\theta d\theta} \ , \end{aligned} \tag{27}$$

see Kinsler et al. [8], Sec.8.9. By Eqs. (2) and (24) it holds that $V(0) = \frac{1}{2}a^2 V_s$, and

$$\int_0^{\pi/2} |V(k\sin\theta)|^2 \sin\theta d\theta = \frac{1}{2\pi\rho_0 ck^2} \Re[P] \ . \tag{28}$$

Consider the case that $ka \to 0$. In [2] it is derived that $\Re[P] \approx \frac{1}{2}\pi\rho_0 c V_s^2 a^2 (ka)^2$. Therefore, as $ka \to 0$

$$D \approx \frac{2(\frac{1}{2}a^2 V_s)^2}{\frac{1}{2\pi\rho_0 ck^2}\frac{1}{2}\pi\rho_0 c V_s^2 a^2 (ka)^2} = 2\ , \tag{29}$$

or 3 dB; this limiting value 2 of D is also found in the case of a rigid piston [8] or a hemispherical source on an infinite baffle.

Next consider the case that $ka \to \infty$. It is shown in [2][Sec. V.D] that

$$\begin{aligned} D &\approx \frac{2(\frac{1}{2}a^2 V_s)^2}{\frac{1}{2\pi\rho_0 ck^2} 2\pi\rho_0 c a^2 \int_0^1 |v(a\rho)|^2 \rho d\rho} \\ &= \frac{\frac{1}{2}(ka)^2 V_s^2}{\int_0^1 |v(a\rho)|^2 \rho d\rho} = C_v (ka)^2\ , \end{aligned} \tag{30}$$

in which C_v is the ratio of the square of the modulus of the average velocity and the average of the square of the modulus of the velocity (averages over S). In case that $v = v^{(\ell)}$, the last member of Eq. (30) is given by $(2\ell+1)(\ell+1)^{-1}(ka)^2$; in Kinsler et al. [8], end of Subsec. 8.9. this result for the case $\ell = 0$ is given.

5 Estimating velocity profiles from on-axis radiation data for far-field loudspeaker assessment

5.1 Estimating velocity profiles from on-axis radiation

The on-axis expression Eqs. (11)–(12) for the pressure can, in reverse direction, be used [1] to estimate the velocity profile on the disk from (measured) on-axis data via its expansion coefficients u_n. This can be effectuated by adopting a matching approach in which the coefficients u_n in the 'theoretical' expression

Eqs. (11)–(12) are determined so as to optimize the match with measured data at $M+1$ points. Thus, one has for the pressure $p_m = p((0,0,r_m))$ due to the velocity profile $v(\sigma) = V_s \sum_{n=0}^{N} u_n R_{2n}^0(\sigma/a)$ the expression

$$\begin{aligned} p_m = \quad & \tfrac{1}{2}\rho_0 c V_s (ka)^2 \cdot \\ & \textstyle\sum_{n=0}^{N} (-1)^n j_n(kr_{m,-}) h_n^{(2)}(kr_{m,+}) u_n \ , \end{aligned} \tag{31}$$

where $r_m \geq 0$ and

$$r_{m,\pm} = \frac{1}{2}(\sqrt{r_m^2 + a^2} \pm r_m) \ , \tag{32}$$

and $m = 0, 1, \cdots, M$. With

$$\begin{aligned} & A = (A_{mn})_{\substack{m=0,1,\cdots,M, \\ n=0,1,\cdots,N}} \ ; \\ & A_{mn} = \tfrac{1}{2}\rho_0 c V_s (ka)^2 j_n(kr_{m,-}) h_n^{(2)}(kr_{m,+}) \ , \end{aligned} \tag{33}$$

$$\underline{p} = [p_0, \cdots, p_M]^T \ , \quad \underline{u} = [u_0, \cdots, u_N]^T \ , \tag{34}$$

the relation between on-axis pressures p_m and coefficients u_n can be concisely written as

$$A\underline{u} = \underline{p} \ . \tag{35}$$

Now given a (noisy) on-axis data vector $\underline{p}$ one can estimate the coefficients vector $\underline{u}$ by adopting a least mean-squares approach for the error $A\underline{u} - \underline{p}$. This will be illustrated by a simulated experiment and, subsequently, by a real experiment, below. In the simulated experiment, we assume a loudspeaker with a Gaussian velocity profile ($\alpha = 2$), as shown in Fig. 8-a curve v_G (dash-dotted).This profile is approximated using three Zernike coefficients (u_0 =0.4323, u_1 =-0.4060, u_2=0.1316), and this leads to the velocity profile v_a (solid curve) in Fig. 8-a. It can be seen from Fig. 8-a that including three Zernike terms provides a fair

approximation (3 10^{-2} absolute accuracy on the whole range). Using the three coefficients of the approximated velocity profile, the sound pressure was calculated by applying Eq. (11) and plotted in Fig. 8-b as p_{calc} (solid curve). Then random white noise was added to p_{calc} as shown as p+noise in Fig. 8-b (dotted curve). Subsequently, the inversion procedure was followed by using the noisy pressure data vector $\underline{p}$ to estimate the coefficients vector $\underline{u}$ by adopting a least mean-squares approach for the error $A\underline{u} - \underline{p}$ (see Eq. (35)). Using the recovered three Zernike coefficients the velocity profile and pressure data were calculated and plotted in Fig. 8-a (thick dotted curve) and Fig. 8-b (thick dotted curve), respectively. It appears that the inversion procedure is rather robust against noise since the calculated and recovered pressure curves in Fig. 8-b are almost coincident.

For the second experiment we measured a loudspeaker (Vifa MG10SD09-08, $a = 3.2$ cm) in an IEC-baffle [16], with the microphone placed at various positions on a straight line at 10 near-field points at zero degree observation angle ($\underline{r}_m$ =0.00, 0.01, 0.02, 0.03, 0.04, 0.05, 0.07, 0.10, 0.13, 0.19 m), and finally the bottom curve for the far-field at 1 m distance. The SPL is plotted in Fig. 9. Figure 9 clearly shows that the near field differs form the far field, in particular at higher frequencies. The lower curve is somewhat noisy because the amplification of the microphone amplifier was kept the same for all measurements.

For a particular frequency at 13.72 kHz ($ka = 8.0423$), the magnitude of the sound pressure is plotted in Fig. 10 (solid curve 'p meas'). Using the same procedure as described above for the first simulation, the inverse process was

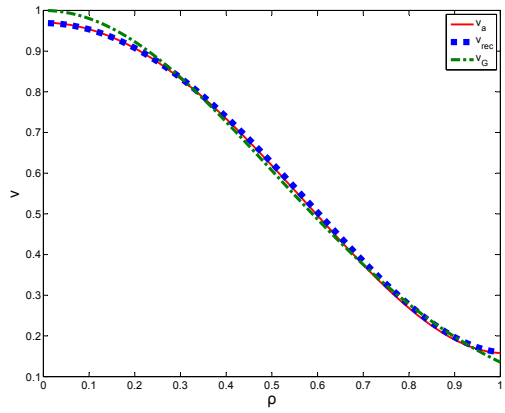

(a)

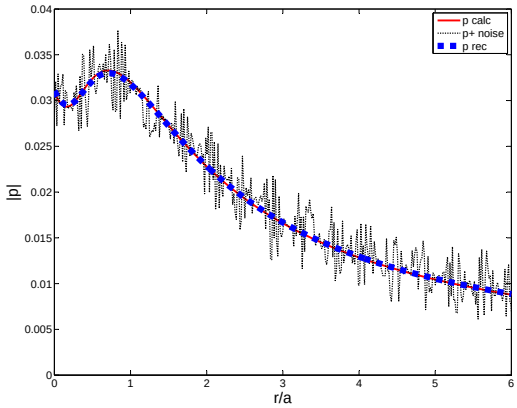

(b)

Figure 8: Simulated experiment. (a) Gaussian velocity profile ($\alpha = 2$) v_G vs. ρ (dash-dotted curve. Approximated velocity profile v_a, Zernike series expansion of [1], Appendix A truncated at $n = 2$ (solid curve). From noisy pressure data recovered velocity profile v_{rec} (thick dotted curve). (b) Sound pressure using Eq. (11) and $ka = 8$ (p_{calc}, solid curve). Pressure with added noise (p+noise, dotted curve). Recovered pressure data (p_{rec} thick dotted curve). Note that the solid curve is almost coincident with the p_{rec} thick dotted curve, but is visible between the dots of that thick curve.

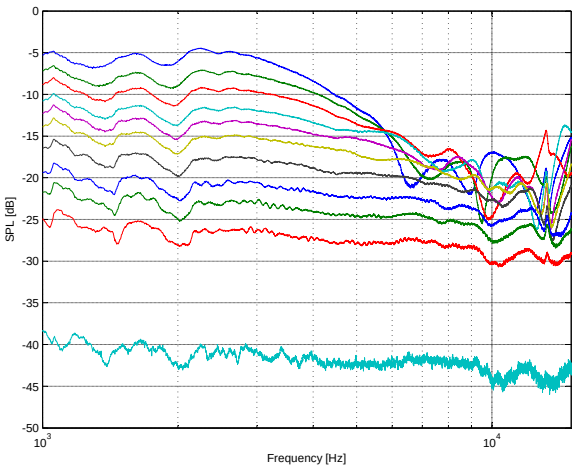

Figure 9: Measured SPL (with arbitrary reference level) for the loudspeaker (Vifa MG10SD09-08, $a = 3.2$ cm) in an IEC-baffle [16], at 10 near-field positions from upper curve (0.00, 0.01, 0.02, 0.03, 0.04, 0.05, 0.07, 0.10, 0.13, 0.19 m), and finally the bottom curve for the far-field at 1 m distance.

followed by using the ten measured near-field pressure data points to estimate the coefficients vector $\underline{u}$. Using four Zernike coefficients the pressure data were recovered and plotted in Fig. 10 (dotted curve 'p rec'). It appears that the two curves show good resemblance to each other and that only four coefficients are needed to provide a very good description of the near-field at rather high frequencies (13.72 kHz). Furthermore, it appears that using these four coefficients, the calculated sound pressure level at 1-m distance yields -42 dB. The measured value at that far-field point is -44 dB. These values match rather closely, even though the cone vibrates not fully circularly symmetric anymore at the used frequency of 13.72 kHz, due to break-up behavior. This match provides a proof of principle as the far-field measurement point was not used to determine the Zernike coefficients, also see Sec. B below.

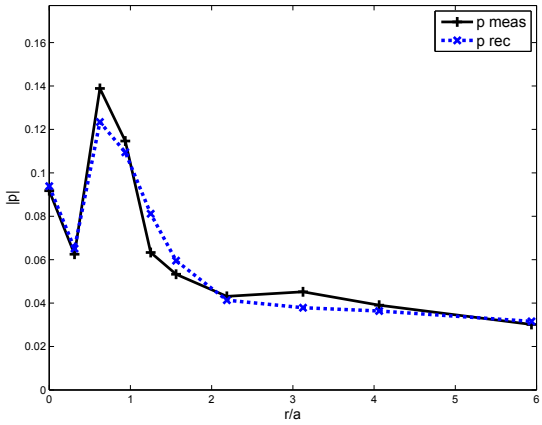

Figure 10: Sound pressure radiated [a.u.] by the loudspeaker that was measured at 13.72 kHz ($ka = 8.0423$, p meas, solid curve) vs. r/a. Recovered pressure data (p rec dotted curve).

In the experiments just described, no particular effort was spent in forming and handling the linear systems so as to have small condition numbers. The condition numbers, the ratio of the largest and smallest non-zero singular value of the matrix A in Eq. (33), equals 50 in the case of the loudspeaker experiment leading to Fig. 10. In practical cases the number of required Zernike coefficients will be less than, say, six. This will not cause numerical difficulties. Furthermore, such a modest number of coefficients already parameterizes a large set of velocity profiles.

5.2 Far-field assessment from on-axis measurements

In Keele [9] a method is described to assess low-frequency loudspeaker performance in the on-axis far-field from an on-axis near-field measurement. In the case of the rigid piston, the on-axis pressure $p(r) = p((0,0,r))$ is given by Eq. (14). Now assume $ka \ll 1$. When $r \ll a$ it holds that

$$\sin(\frac{1}{2}k(\sqrt{r^2+a^2}-r)) \approx \sin(\frac{1}{2}ka) \approx \frac{1}{2}ka \quad , \tag{36}$$

and, when $r \gg a$ it holds that

$$\sin(\frac{1}{2}k(\sqrt{r^2+a^2}-r)) \approx \sin(\frac{ka^2}{4r}) \approx \frac{ka^2}{4r} \quad . \tag{37}$$

Therefore, the ratio of the moduli of near-field and far-field on-axis pressure is given by $2r/a$. This is the basis of Keele's method; it allows far-field loudspeaker assessment without having to use an anechoic room.

With the inversion procedure to estimate velocity profiles from on-axis data (which are taken in the relative near-field) as described in Sec. 5.1 together

with the forward calculation scheme for the far-field as described in Sec. 3.2, it is now possible to generalize Keele's scheme. This is illustrated by comparing the far-field responses pertaining to the two sets of Zernike coefficients occurring in the Gaussian simulated experiment, see Fig. 8 in Sec. 5.1. Using Eq. (19) the normalized far-field pressure is plotted in Fig. 11 as p_{calc} (solid curve) and p_{rec} (dotted) curve, respectively ($\alpha = 2, ka = 8$), where the normalization is such that the factor in front of the series at the right-hand side of Eq. (19) equals unity. It appears that the two curves are very similar. This confirms that the u_n obtained from the noisy near-field measured pressure data yield a good estimate of the far-field spatial pressure response.

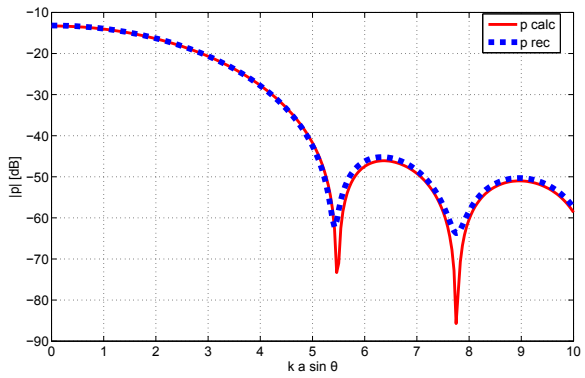

Figure 11: Simulated experiment Gaussian radiator ($\alpha = 2$). Normalized sound pressure in the far-field using Eq. (19) and $ka = 8$ (p_{calc}, solid curve). Recovered normalized far-field pressure data (p_{rec}dotted curve).

6 Discussion and outlook

This paper has considered a method to perform forward and inverse sound pressure computations for circular radiators with a non-uniform velocity profile. However, it must be stated that not all drivers move in a circularly symmetric fashion. Shallow cones have significant circumferential modes. For example, automotive loudspeakers and transducers without spider (headphones and microspeakers) suffer from rocking modes. This needs further research.

In the forward problem, the velocity profile is assumed to be known and the on-axis and far-field sound pressure are expressed analytically in terms of Zernike expansion coefficients of the velocity profile and (spherical) Bessel (and Hankel) functions. In the inverse problem, the velocity profile is unknown and is estimated in terms of Zernike expansion coefficients from on-axis pressure data by adopting a matching approach based on the analytic result for the on-axis pressure. Well-behaved velocity profiles are already adequately represented by only a few terms of their Zernike expansion. Therefore, the Zernike series approach is more convenient for both the forward problems and the inverse problem than, for instance, an approach based on expansions involving the family of rigid, simply supported and clamped radiators. The forward and inverse method is proposed for use in assessment of the far-field of a loudspeaker without the need for an anechoic room. Here, the Zernike coefficients of the velocity profile are estimated from the on-axis (relatively near-field) data, and these coefficients are used in the forward scheme to compute the far-field. This assessment procedure has not been fully worked out in the present paper due to

a variety of practical issues that need to be addressed. Among these practical issues are

- choice of the on-axis measurement points,
- condition of the linear systems that arise,
- influence of ka,
- influence of noise,
- influence of misalignment of the measurement points,
- influence of inclination of the measurement axis,
- incorrect setting of the radius of the radiator,
- accuracy of the identified velocity profile and the role of this intermediate result,

while various combinations of these issues should also be considered. It can already be said that in practice the number of retrieved Zernike coefficients will be in the order of five. The real number will be depending on the condition number of the matrix A in Eq. (35). The authors intend to work out the method for the loudspeaker assessment with attention for the above mentioned points.

In this paper, the theory has been developed for flat radiators. However, the basic result for the on-axis pressure as a series expansion, in terms of Zernike coefficients and spherical Bessel and Hankel functions, has been generalized to the case of dome-shaped radiators [1]. Furthermore the theory is adapted to

spherical loudspeaker cabinets, where the loudspeaker is modelled as a moving cap on the sphere [11]. It is, therefore, to be expected that both the forward and the inverse methods can also be generalized to the case of dome-shaped radiators. The authors intend to develop the method both on a theoretical and practical level for dome-shaped radiators as well.

7 Conclusions

Zernike polynomials are an efficient and robust method to describe velocity profiles of resilient sound radiators. A wide variety of velocity profiles, including the rigid piston, the simply supported radiator, the clamped radiators, Gaussian radiators as well as real loudspeaker drivers, can be approximated accurately using only a few terms of their Zernike expansions. This method enables one to solve both the forward as well as the inverse problem. With the forward method the on-axis and far-field off-axis sound pressure are calculated for a given velocity profile. With the inverse method the actual velocity profile of the radiator is calculated using (measured) on-axis sound pressure data. This computed velocity profile allows the extrapolation to far-field loudspeaker pressure data, including off-axis behavior, without the use of anechoic rooms.

References

[1] R.M. Aarts and A.J.E.M. Janssen. On-axis and far-field sound radiation from resilient flat and dome-shaped radiators. *J. Acoust. Soc. Am.*, 125(3), 1444-1455, March 2009.

[2] R.M. Aarts and A.J.E.M. Janssen. Sound radiation quantities arising from a resilient circular radiator. *J. Acoust. Soc. Am.*, 126(4), 1776–1787, Oct. 2009.

[3] B.R.A. Nijboer. *The diffraction theory of aberrations.* Ph.D. dissertation, University of Groningen, The Netherlands, 1942.

[4] F. Zernike and B.R.A. Nijboer. The theory of optical images (published in French as La théorie des images optiques). *Revue d'Optique*, Paris, page 227, 1949.

[5] M. Born and E. Wolf. *Principles of Optics*, 7th ed. Cambridge University Press, Cambridge, Chap. 9, 2002.

[6] J.J.M. Braat, S. van Haver, A.J.E.M. Janssen, and P. Dirksen. Assessment of optical systems by means of point-spread functions. In *Progress in Optics* (Vol. 51) edited by E. Wolf (Elsevier, Amsterdam), Chap. 6, 2008.

[7] M. Greenspan. Piston radiator: Some extensions of the theory. *J. Acoust. Soc. Am.*, 65, 608–621, 1979.

[8] L.E. Kinsler, A.R. Frey, A.B. Coppens, and J.V. Sanders. *Fundamentals of Acoustics.* Wiley, New York, 1982.

[9] D.B. (Don) Keele, Jr. Low-frequency loudspeaker assessment by nearfield sound-pressure measurement. *J. Audio Eng. Soc.*, 22(3), 154–162, April 1974.

[10] J.W.S. Rayleigh. *The Theory of Sound, Vol. 2, 1896.* (reprinted by Dover, New York), 1945.

[11] R.M. Aarts and A.J.E.M. Janssen. Modeling a loudspeaker as a resilient spherical cap on a rigid sphere. 128th AES Convention London May 20–23, 2010.

[12] F.J.M. Frankort. *Vibration and Sound Radiation of Loudspeaker Cones.* Ph.D. dissertation, Delft University of Technology, 1975.

[13] M. Abramowitz and I.A. Stegun. *Handbook of Mathematical Functions.* Dover, New York, 1972.

[14] H. Stenzel. On the acoustical radiation of membranes (published in German as Über die Akustische Strahlung von Membranen). *Ann. Physik*, 7, 947–982, 1930.

[15] L.V. King. On the acoustic radiation field of the piezo-electric oscillator and the effect of viscosity on transmission. *Can. J. Res.*, 11, 135–155, 1934.

[16] International Electrotechnical Commission (IEC), Geneva, Switzerland. IEC 60268-5 Sound System Equipment - Part 5: Loudspeakers, 2007

List of Figures

List of Tables

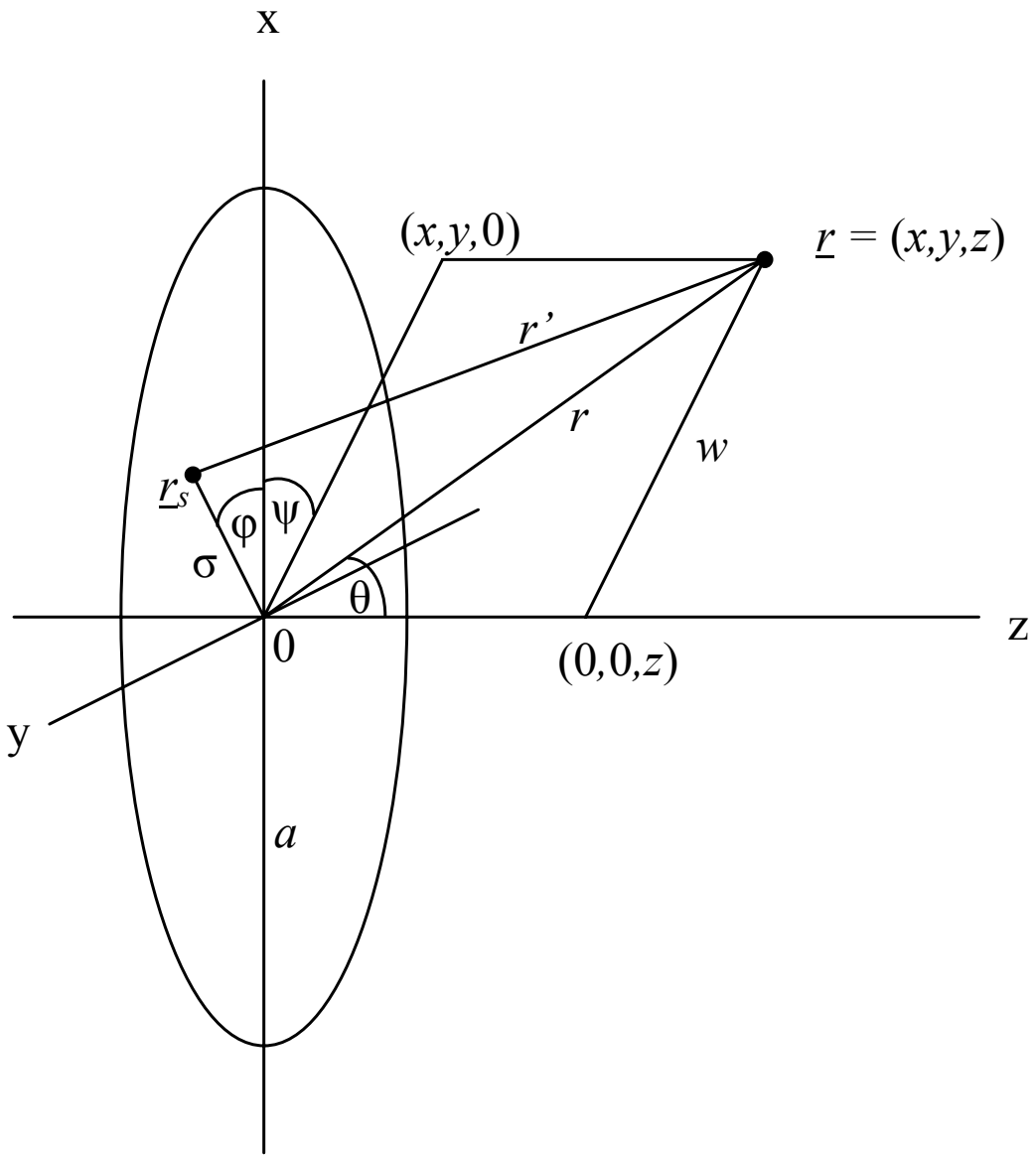

Fig. 1 Set-up and notations.

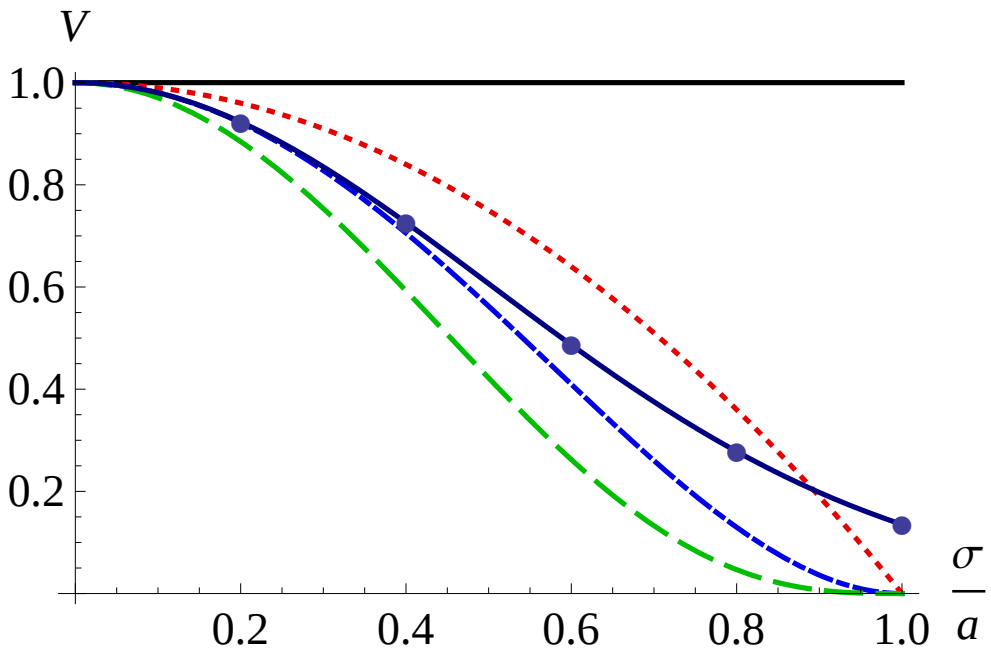

Fig. 2

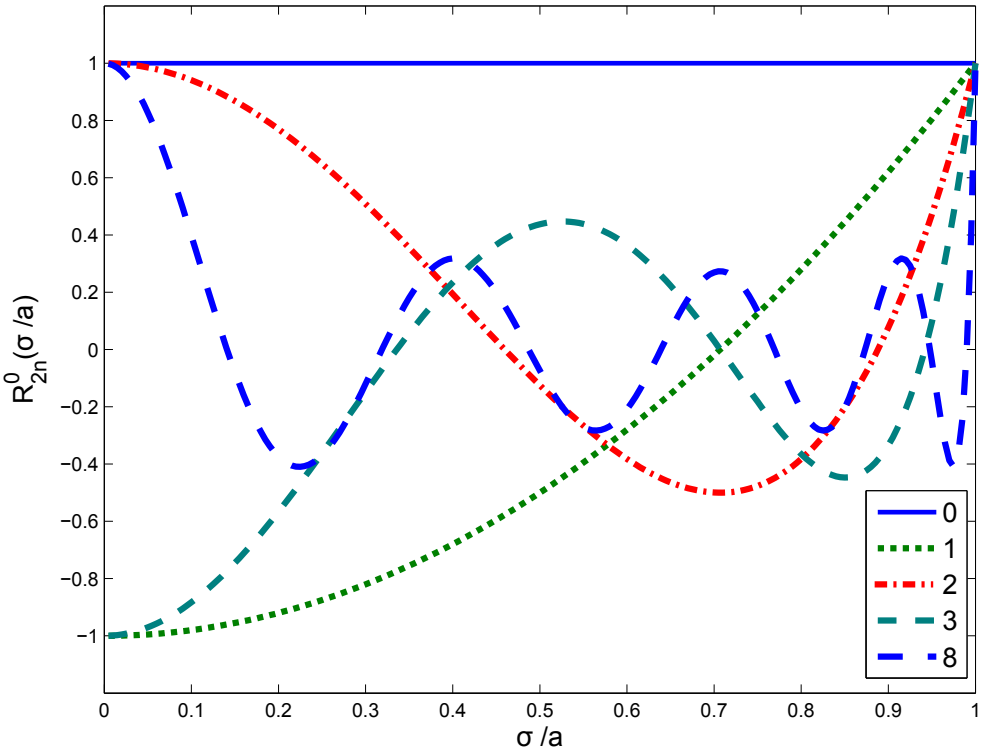
1
0.8
0.6
0.4
0.2
0
−0.2
−0.4
−0.6
−0.8
−1
0
0.1
0.2
0.3
0.4
0.5
0.6
0.7
0.8
0.9
1
σ /a
$R^0_{2n}(\sigma/a)$
0
1
2
3
8

Fig. 3

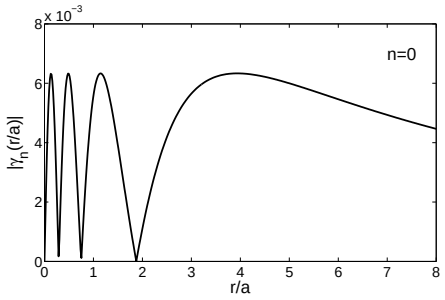

(a)

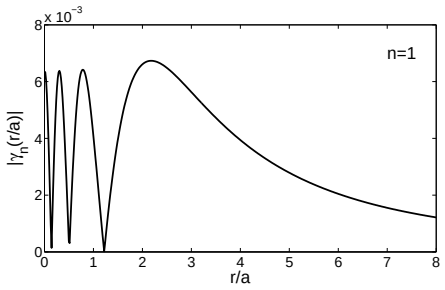

(b)

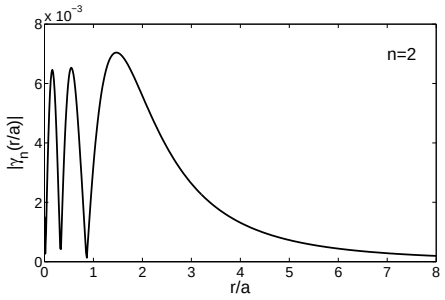

(c)

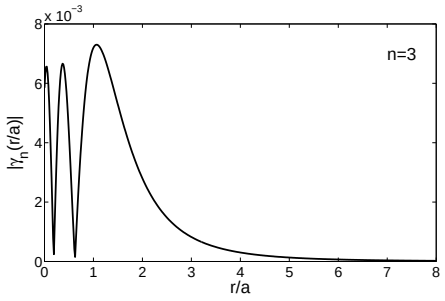

(d)

Fig. 4

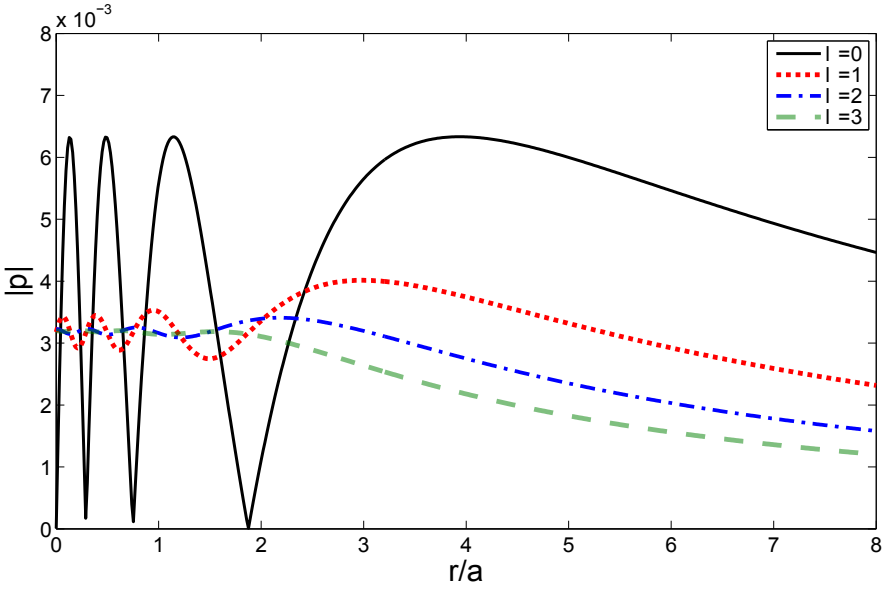

Fig. 5

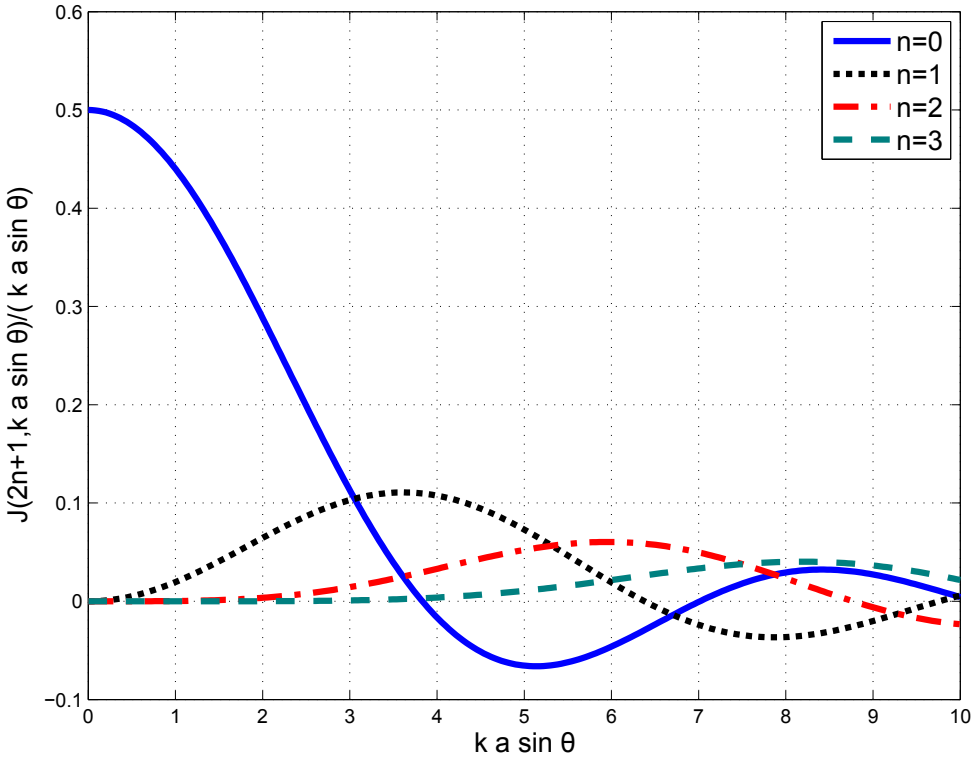
n=0
n=1
n=2
n=3
J(2n+1,k a sin θ)/(k a sin θ)
k a sin θ
0.6
0.5
0.4
0.3
0.2
0.1
0
−0.1
0
1
2
3
4
5
6
7
8
9
10

Fig. 6

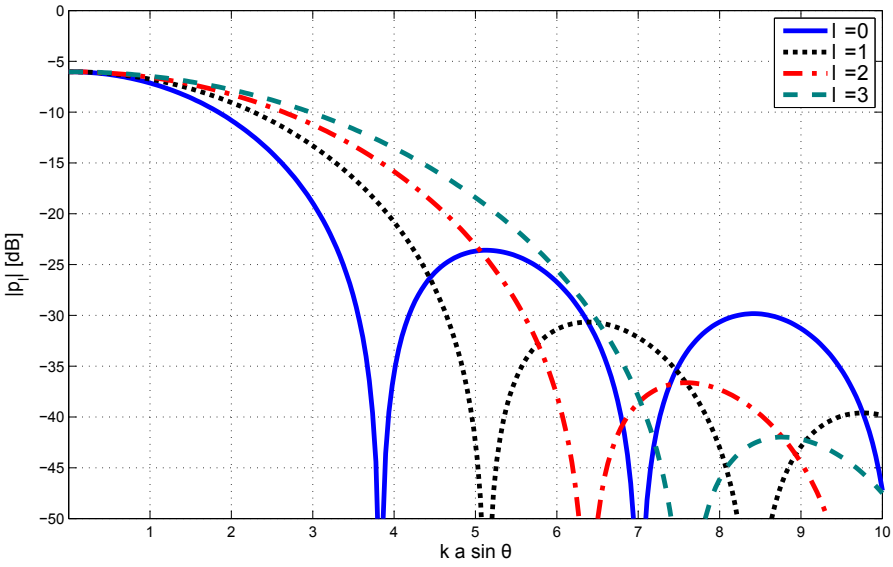

Fig. 7

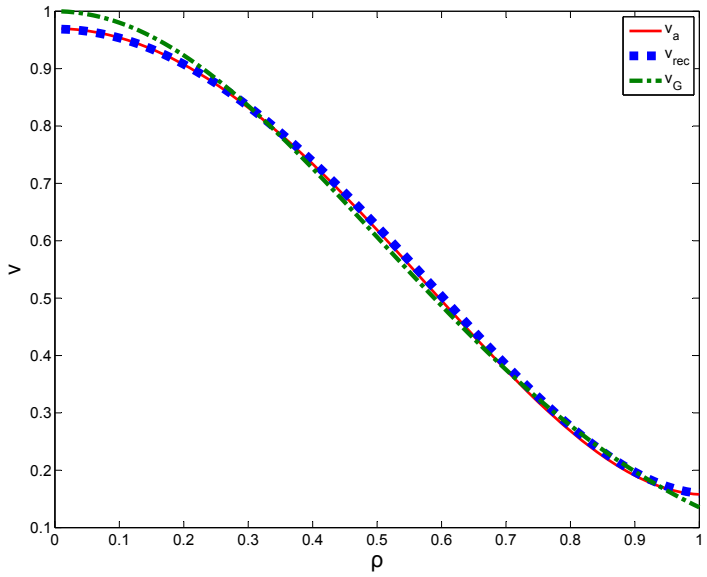

(a)

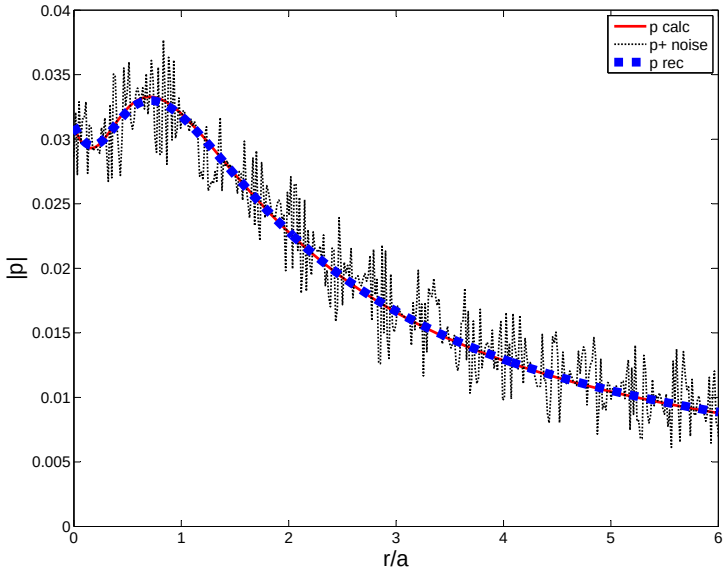

(b)

Fig. 8

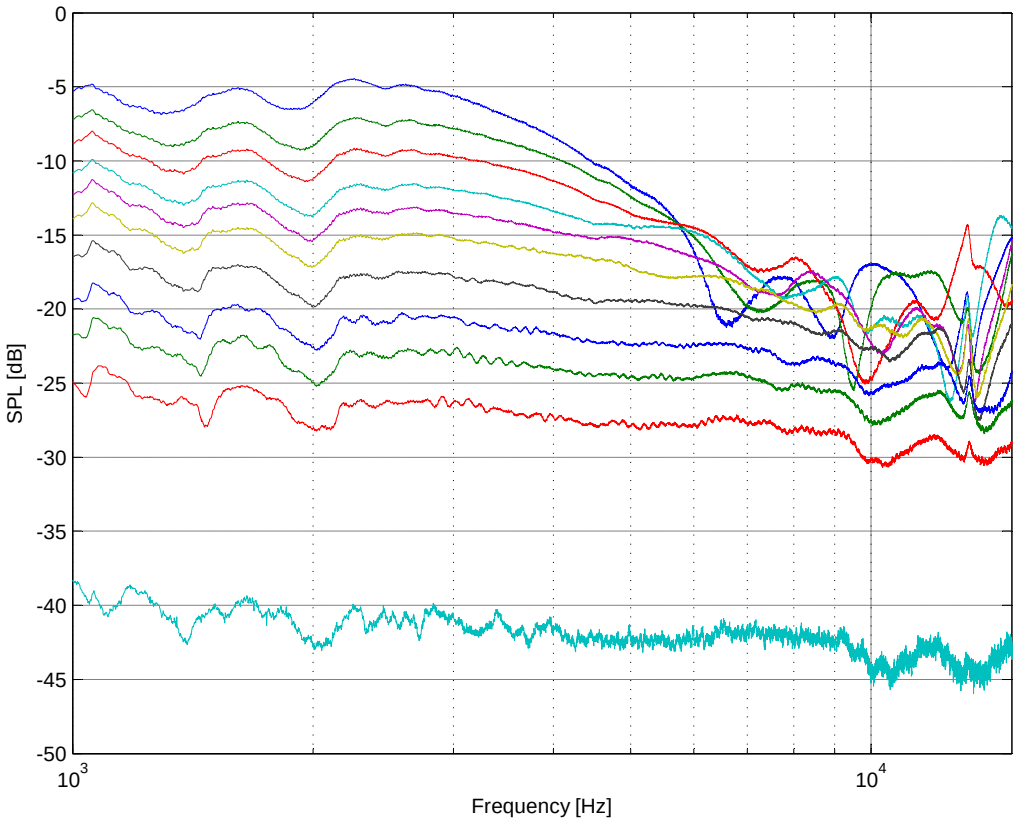

Fig. 9

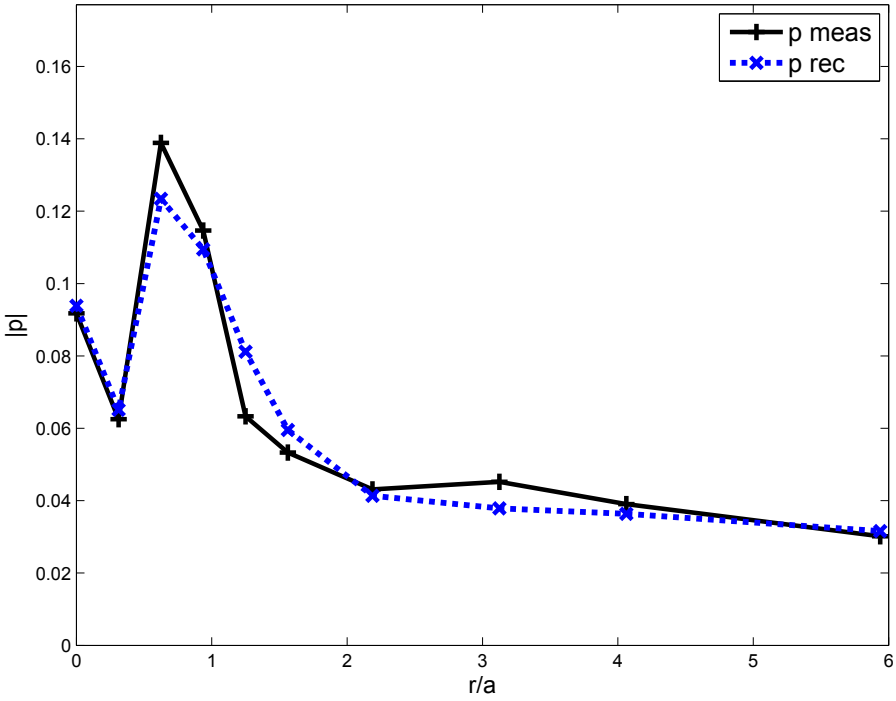

Fig. 10

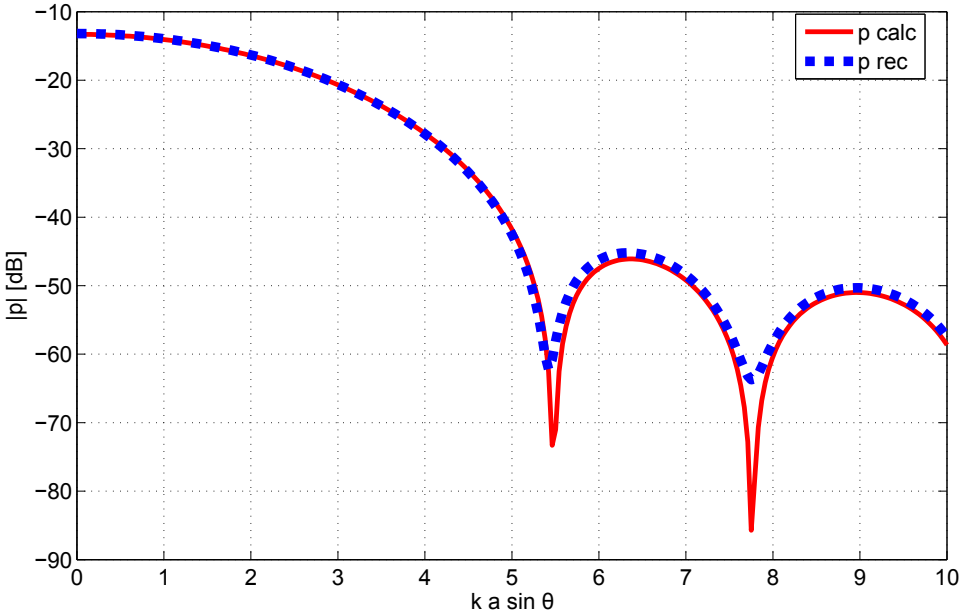

Fig. 11